A tunable microwave plasma photonic crystal filter

Cite as: Appl. Phys. Lett. **107**, 171107 (2015); https://doi.org/10.1063/1.4934886
Submitted: 20 July 2015 . Accepted: 16 October 2015 . Published Online: 29 October 2015

B. Wang, and M. A. Cappelli

A tunable microwave plasma photonic crystal filter

B. Wang and M. A. Cappelli
Stanford Plasma Physics Laboratory, Department of Mechanical Engineering, Stanford University, Stanford, California 94305, USA

(Received 20 July 2015; accepted 16 October 2015; published online 29 October 2015; corrected 30 October 2015)

The integration of gaseous plasma elements into a microwave photonic crystal band gap cavity structure allows for active tuning of the device. An alumina rod array microwave photonic crystal waveguide resonator is simulated and characterized through finite difference time domain methods. A gaseous plasma element is integrated into the cavity structure and the effect of plasma density on the transmission properties of the structure is investigated. We show, through both simulations and experiments, that the permittivity of the plasma can be adjusted to shift the peak resonance to allow for both switching and tunability of transmission. The experimentally measured peak shifts in transmission are compared to those simulated and the electron density of the gaseous plasma element is calculated and compared to values determined from the measured discharge current density. © *2015 AIP Publishing LLC*. [http://dx.doi.org/10.1063/1.4934886]

Photonic crystal band gap devices are now commonly used for manipulating radiation sources.[1,2] These types of devices have been shown to be useful in the control of electromagnetic (EM) waves in the microwave,[3] terahertz,[4] and optical regions[5] of the EM spectrum. Devices such as filters, couplers, switches, and modulators have been designed.[6,7] The use of gaseous plasma elements in such structures has been of recent interest due to the plasmas' dispersive properties, tunable permittivity in both the positive and negative regimes, and active switching capabilities.[8] Plasmas can be generated through radio frequency (RF),[9] direct current (DC),[10] and alternating current (AC)[11] methods and have been shown to have a plasma frequency that is high enough to affect the propagation of microwave frequency radiation.[12] The integration of plasma elements into photonic crystal band gap devices allows for active tunability and control of transmission properties;[13,14] however, few devices have been experimentally fabricated and characterized. Resonance cavity diagnostic methods for measuring plasma density have been used for plasma diagnostics.[15] Here, we extend the concept by integrating tunable plasma elements into a resonance cavity of a microwave photonic crystal.

In this letter, we present computations and measurements of the performance of a photonic crystal cavity bandpass filter containing a functionalized plasma element that has a tunable transmission peak within the passband frequency. Finite-difference time-domain (FDTD) simulations are used to predict the effects of changing plasma density on the transmission spectrum of the device. An experimental device is fabricated, characterized, and compared to the simulated performance.

Figure 1 is a schematic of the plasma photonic crystal device and serves to illustrate both the basic structure that is simulated, as well as the experimental configuration. The device has a two-dimensional (2D) structure with an input waveguide on the left and right of a resonant cavity. The starting point is that of a photonic crystal consisting of an 11×9 array of alumina rods ($\varepsilon = 9.4$) of diameter $d = 3$ mm in air on a square lattice with a lattice constant of $a = 10$ mm. The photonic crystal supports transverse magnetic (TM) mode propagation with a band gap between 11 and 15 GHz. An input and output waveguide can be formed by removing a row of rods, allowing for transmission within the bandgap. A partial waveguide is formed by removing the two outermost rods along a row, and a tunable resonant cavity is formed by removing the three central rods along the same row and by placing a plasma discharge element of diameter $d = 13$ mm and a 1 mm thick quartz envelope ($\varepsilon = 3.8$) in the center rod location. Two passbands are formed with this arrangement, a lower frequency passband centered at 13.8 GHz and a higher frequency secondary passband that is centered at 14.2 GHz. The lower passband peak is functionalized by the plasma. Adding a plasma cylinder in the center of the cavity allows for tunability of the lower passband resonance frequency through adjustment of the plasma density (n_e) and hence the plasma permittivity. The plasma permittivity is represented with a usual Drude model

$$\varepsilon_p(\omega) = 1 - \frac{\omega_p^2}{\omega^2 - i\gamma\omega}, \tag{1}$$

where γ is the electron momentum transfer collision frequency. The plasma frequency

$$\omega_p = \sqrt{\frac{n_e e^2}{m_e \varepsilon_0}}. \tag{2}$$

Here, e is the electron charge, m_e is the electron mass, ω is the EM field frequency, and ε_o is the free space permittivity. The plasma density, and thus, the plasma frequency and permittivity are tunable in various plasmas by controlling parameters such as the gas composition, pressure, electrode bias voltage, and discharge current. We simulate the plasma as collisionless as well as with collisions to understand the effects of collisions on the transmission peaks. A brief discussion about the possible effects of electron collisions on the EM wave transmission properties is discussed later in the letter.

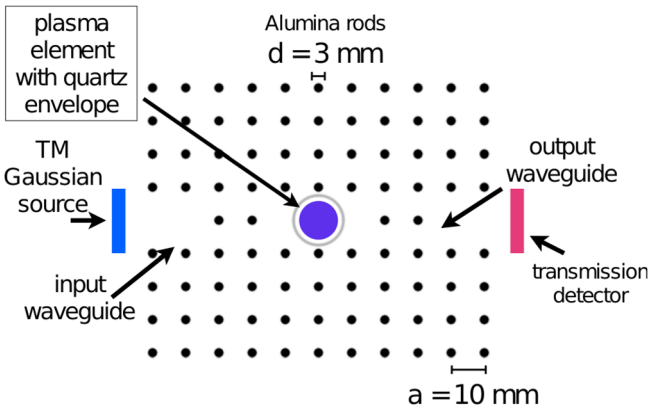

FIG. 1. Schematic of plasma photonic crystal resonance cavity structure. The black circles are alumina rods, with a single plasma element represented by the purple circle. A 1 mm thick circular quartz envelope encloses the plasma element.

An open source finite-difference time-domain simulation (MEEP)[16] is used to compute the 2D EM wave transmission and to visualize the fields in the device. Propagating modes were excited with a Gaussian pulse located at the input waveguide and the resulting transmission coefficient was calculated from the transmitted energy flux at the output waveguide. The FDTD simulation requires a specification of the plasma density distribution within the plasma tube. The plasma experiences radial diffusion due to wall recombination with a radial electron density distribution that is expected to be near parabolic in shape. To simplify the simulation, we distribute the plasma electrons uniformly over a diameter that is $1/\sqrt{2}$ times the inner discharge tube diameter (plasma diameter of 9.2 mm), with an electron density that is twice that if the electrons were distributed uniformly over the entire tube diameter of d = 13 mm. In this letter, we refer to the cross sectional averaged plasma density as $\overline{n_e}$, which is the averaged electron density over the cross section of the entire tube diameter.

Figure 2 shows the results of the FDTD simulations describing the effect that variations in plasma density have on the transmission spectra of the device. For the results shown in the figure, we treat the plasma to be collisionless. We see that the resonance frequency of the tunable peak shifts towards higher frequency as the plasma density is increased. The device shows fine tunability on the order of tens of MHz when adjusting the plasma density in the range of $\overline{n_e} = 10^{11}$ cm^{-3} to $\overline{n_e} = 7 \times 10^{11}$ cm^{-3}. The secondary resonance mode at 14.2 GHz shifts slightly but is not greatly affected by the change in the plasma density. It is noteworthy that at a plasma density of about $\overline{n_e} = 6 \times 10^{11}$ cm^{-3}, the tunable peak shifts enough to overlap with the secondary resonance peak. This particular operating condition is potentially useful as the fast switch or modulation of radiation centered on the passband frequency near 13.8 GHz if the plasma can be turned on or off, or modulated, at high rates.

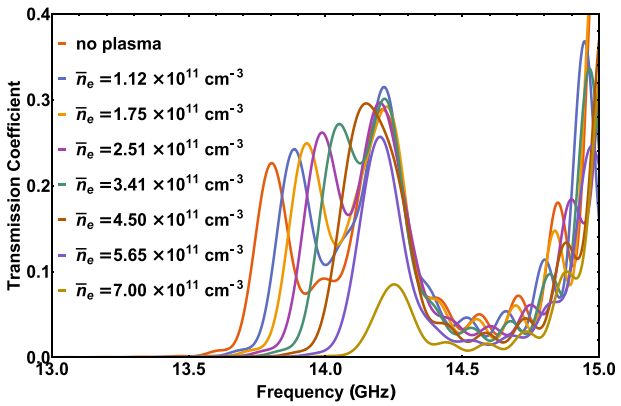

FIG. 2. Simulated transmission spectra for the plasma photonic crystal cavity device for various plasma densities, with a collisionless plasma column of diameter d = 9.2 mm.

The designed device was fabricated using 150 mm long alumina rods (99.6% purity) supported by an acrylic frame. A 15 mm diameter quartz tube with a inner wall thickness of 1 mm and length of 290 mm, filled with argon to 250 Pa and mercury, serves as the discharge plasma. The discharge temperature was estimated to be around 330 K,[17] giving a mercury vapor partial pressure of about 3.5 Pa.[18] The discharge was driven by an AC ballast with a peak to peak voltage of 160 V. The voltage waveform was triangular in shape resulting in a root-mean-square (RMS) voltage of $V_{RMS} = 46.2$ V. The ballast had a variable peak current (also close to triangular in wave form) ranging from 24.8 mA to 111.1 mA, with a ballast frequency that decreased linearly from 55.0 kHz to 37.0 kHz for increasing peak current in the range from 24.8 mA to 51.2 mA, and a ballast frequency in the range of 32.2 kHz–33.8 kHz for peak discharge currents from 54.4 mA to 111.2 mA. Two broad band (2 GHz–18 GHz) microwave horns are used as the source and detector, connected to an HP 8722D Vector Network Analyzer to measure the transmission coefficient of the device. The measured transmission was recorded with an integration time of 5 ms. This integration time is enough to average the transmission over several excursions in plasma density as the plasma density is also expected to oscillate at the driven AC frequency. Figure 3 shows the experimental setup with the horn antennas, acrylic support frame, and the photonic crystal with the plasma discharge ignited.

Figure 4 shows the experimental transmission spectra as a function of the peak discharge current. As the discharge current is increased, the concomitant increase in plasma

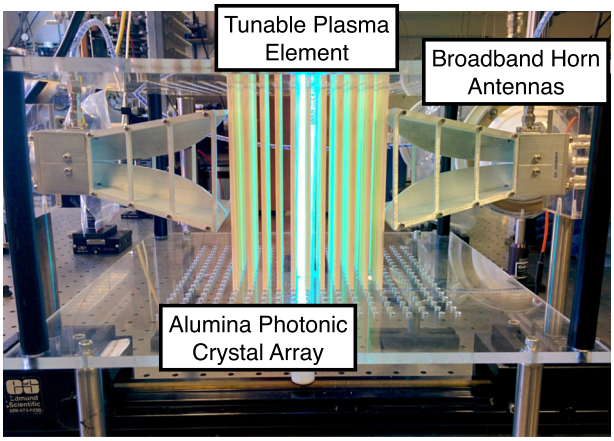

FIG. 3. Experimental setup with alumina photonic crystal array, tunable plasma discharge, and measurement setup. An acrylic base structure is used to support the device.

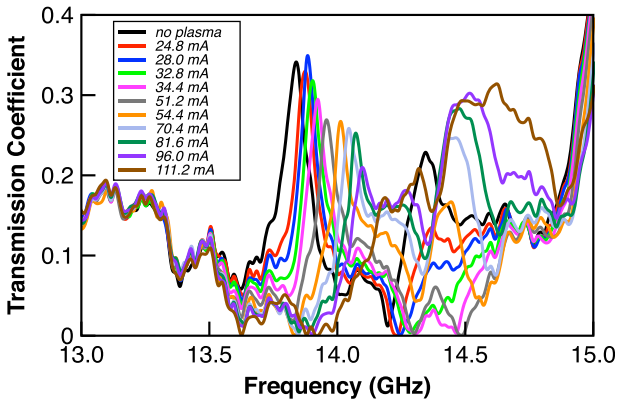

FIG. 4. Experimental transmission spectra for the plasma photonic crystal cavity device for various peak plasma discharge currents.

density shifts the peak transmission of the tunable resonance towards higher frequency. At the maximum peak discharge current of 111.2 mA, the transmission peak is shifted into the secondary resonance, and, at the resonance frequency in the absence of a plasma, i.e., at 13.8 GHz, the transmission coefficient is found to be less than 0.05. The reduction in the peak of the transmission coefficient with increased discharge current is attributed to the possible role played by electron scattering collisions. Collisions tend to broaden and lower the peak transmission (as a result of attenuation losses) and the quality (Q) of the resonant cavity.

Figure 5 depicts the measured peak frequency shift as a function of the RMS current, I_{RMS}. Also shown in the figure, for comparison, is the simulated peak frequency shift versus plasma density (averaged over the entire 13 mm diameter of the discharge). The dashed line is a linear fit through the simulated values. The correspondence between the two curves allows for an estimate of this averaged plasma density (see solid black circles in Fig. 6), within the framework of the assumptions made in the simulations. The major source of experimental uncertainty in this estimate is the repeatability in the measured frequency shift for a given discharge current. The impact on the results from the assumption of a collisionless plasma is discussed below. The upper and lower bound on the frequency measurements provide an estimate

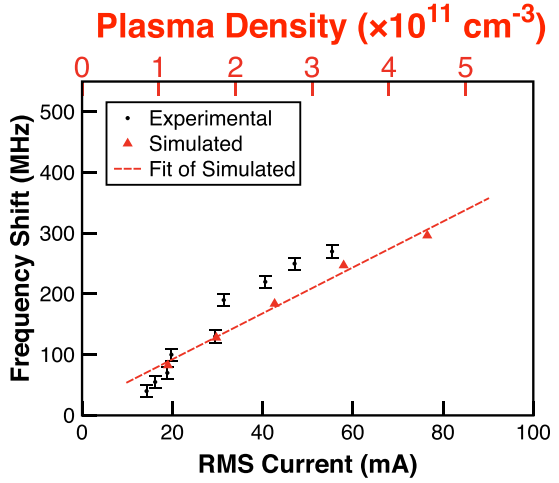

FIG. 5. Experimental transmission peak shift vs. peak plasma discharge current plotted against simulated transmission peak shift vs. plasma density.

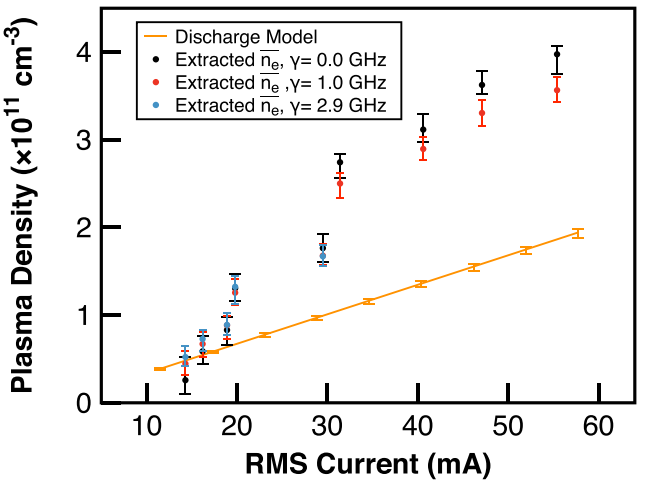

FIG. 6. Experimentally derived plasma density vs. RMS current with the analytically derived plasma density vs. RMS current.

of the uncertainty in the plasma density assignments. Figure 6 shows that the discharge plasma density is estimated to be in the range of $\overline{n_e} = 0.3 \times 10^{11}\text{cm}^{-3}$ to $\overline{n_e} = 4 \times 10^{11}\text{cm}^{-3}$ for this collisionless plasma case.

The reasonableness of the estimated plasma densities extracted from the resonance peak shifts given by the solid black circles in Fig. 6 can be evaluated through the comparison of a simple analysis based on the measured I_{RMS}, the known discharge tube cross-sectional area, A, and the electron drift velocity, u_d. The drift velocity requires an estimate of the time-averaged reduced electric field, the latter of which can be determined from V_{RMS}/L (corrected for an estimated cathode fall voltage of approximately 6–11 V (Ref. 19)), with $L = 177$ mm, the approximate length of the visible discharge positive column (determined from images obtained with a high speed camera). Electron drift velocities for a mixture of argon and mercury were obtained using the electron energy distribution and swarm properties calculator, BOLSIG,[20] for reduced electric field (E/N) values ranging from approximately 3.73 Td to 4.00 Td, assuming that the discharge tube is filled to the specified pressure at a temperature of about 300 K and operates at a temperature of about 330 K.

The modeled averaged electron number density extracted from this simple model analysis, $\overline{n_{em}}$, is derived from

$$\overline{n_{em}} = \frac{I_{RMS}}{eAu_d}. \tag{3}$$

This electron density should be interpreted as a spatial (over the entire tube diameter) and temporal average, as is that which determines the measured resonance shift. The electron density determined by this analysis is given by the solid orange line in Fig. 6. The solid orange line is a least-square fit to the discrete data. Also shown are upper and lower limits based on estimated uncertainties in the properties that enter into determining reduced field at values of current density where data are collected. We see that the tube-averaged plasma density determined from the resonance shift agrees reasonably well with the simple model analysis at low

discharge currents, but is about twice that estimated by the model at the highest current studied.

We partially attribute the discrepancy between the electron density determined by the simple model analysis and that inferred from the resonance shift and FDTD simulations to the assumption about the collisionality of the plasma. The BOLSIG simulations are also used to estimate a total electron momentum transfer collision frequency of approximately 2.9 GHz. The FDTD simulations of the EM wave transmission spectra were reproduced with this estimated collision frequency included in the Drude expression. The resulting plasma densities, mapped onto the discharge current for the collisional case, are added as solid blue circles to Fig. 6. A lower collision frequency of 1.0 GHz was also simulated to see the effect at higher plasma densities, since the higher plasma collision frequency case caused the simulated resonance to be damped and broadened by amounts greater than that seen in the experiments and the peak shift to be buried within the secondary resonance feature. We see that the inclusion of collisions brings the experiments into slightly better agreement with the model analysis. It is noteworthy that electron scattering collisions seem to raise the inferred plasma density at low current density and lower the inferred plasma density at high current density. Collisions seem to reduce the plasma density-driven resonance shift at low plasma densities and enhance it at higher plasma densities. This behavior is attributed to the collision-induced attenuation, and will be examined further as part of a continued study of this plasma photonic crystal device. The remaining discrepancy between experiments and modeling at the higher current density remains to be resolved, although the remaining differences are well within a factor of two. We believe that some of these differences can be attributed to the assumptions of the two dimensionality in the FDTD simulations. Future studies will use three dimensional simulations for more accurate predictions of device performance.

To summarize, we have presented a photonic crystal filter with active tunability through incorporating a functionalized plasma element into the resonator of the device. This plasma photonic crystal is shown to be tunable by changing the plasma density of the plasma element. A methodology is also presented for determining the plasma density of the discharge through measuring experimental shifts in the resonator frequency as a function of plasma discharge current and correlating values to simulated shifts in resonator frequency with known plasma densities. Incorporation of additional plasma elements for more complex tuning schemes and device configurations will be investigated in the future.

This work was supported in part by a Multidisciplinary University Research Initiative from the Air Force Office of Scientific Research. B.W. was also supported in part by a National Defense Science and Engineering Graduate Fellowship.

[1]S. Fan, P. Villeneuve, J. Joannopoulos, and E. Schubert, "High extraction efficiency of spontaneous emission from slabs of photonic crystals," Phys. Rev. Lett. **78**, 3294–3297 (1997).
[2]S. Fan and J. Joannopoulos, "Analysis of guided resonances in photonic crystal slabs," Phys. Rev. B **65**, 235112 (2002).
[3]N. Kaina, F. Lemoult, M. Fink, and G. Lerosey, "Ultra small mode volume defect cavities in spatially ordered and disordered metamaterials," Appl. Phys. Lett. **102**, 2–5 (2013); e-print arXiv:1112.2536.
[4]K. Saito, "THz-wave generation from GaP THz photonic crystal waveguides under difference-frequency mixing," Opt. Photonics J. **02**, 201–205 (2012).
[5]D. Yang, H. Tian, and Y. Ji, "Nanoscale photonic crystal sensor arrays on monolithic substrates using side-coupled resonant cavity arrays," Opt. Express **19**, 20023 (2011).
[6]O. Sakai, J. Maeda, T. Shimomura, and K. Urabe, "Functional composites of plasmas and metamaterials: Flexible waveguides, and variable attenuators with controllable phase shift," Phys. Plasmas **20**, 073506 (2013).
[7]P. Villeneuve, S. Fan, and J. Joannopoulos, "Microcavities in photonic crystals: Mode symmetry, tunability, and coupling efficiency," Phys. Rev. B **54**, 7837 (1996).
[8]O. Sakai and K. Tachibana, "Plasmas as metamaterials: a review," Plasma Sources Sci. Technol. **21**, 013001 (2012).
[9]W. McColl, C. Brooks, and M. L. Brake, "Electron density and collision frequency of microwave-resonant-cavity- produced discharges," J. Appl. Phys. **74**, 3724–3735 (1993).
[10]Y. A. Safronau and L. V. Simonchik, "Non-self-sustained glow discharges in atmospheric-pressure inert and molecular gases in a three-electrode configuration," IEEE Trans. Plasma Sci. **39**, 2098–2099 (2011).
[11]M. K. Howlader, Y. Yang, and J. R. Roth, "Time-resolved measurements of electron number density and collision frequency for a fluorescent lamp plasma using microwave diagnostics," IEEE Trans. Plasma Sci. **33**, 1093–1099 (2005).
[12]T. Anderson and I. Alexeff, "Plasma frequency selective surfaces," IEEE Trans. Plasma Sci. **35**, 407–415 (2007).
[13]L. Dong, H. Xiao, W. Fan, H. Zhao, and H. Yue, "A plasma photonic crystal with tunable lattice constant," IEEE Trans. Plasma Sci. **38**, 2486–2490 (2010).
[14]G.-C. T. G.-C. Tai, Y.-W. K. Y.-W. Kiang, and C. C. C. Chen, "Plasma-dielectric sandwich structure used as a tunable microwave filter," in *Antennas and Propagation Society International Symposium* (1982), Vol. 20, pp. 111–113.
[15]B. Agdur and B. Enander, "Resonances of a microwave cavity partially filled with a plasma," J. Appl. Phys. **33**, 575–581 (1962).
[16]A. F. Oskooi, D. Roundy, M. Ibanescu, P. Bermel, J. D. Joannopoulos, and S. G. Johnson, "Meep: A flexible free-software package for electromagnetic simulations by the FDTD method," Comput. Phys. Commun. **181**, 687–702 (2010).
[17]C. Kenty, M. a. Easley, and B. T. Barnes, "Gas temperatures and elastic losses in low pressure mercury-argon discharges," J. Appl. Phys. **22**, 1006 (1951).
[18]M. L. Huber, A. Laesecke, and D. G. Friend, "The Vapor Pressure of Mercury," NIST Interagency/Internal Report (NISTIR), Report No. NISTIR 6643, 2006.
[19]A. Hilscher, "Determination of the cathode fall voltage in fluorescent lamps by measurement of the operating voltage," J. Phys. D: Appl. Phys. **35**, 1707–1715 (2002).
[20]G. J. M. Hagelaar and L. C. Pitchford, "Solving the Boltzmann equation to obtain electron transport coefficients and rate coefficients for fluid models," Plasma Sources Sci. Technol. **14**, 722–733 (2005).